Influence of FE model variability in predicting brain motion and intracranial pressure changes in head impact simulations

doi:10.1533/ijcr.2004.0299

T J Horgan[1] and M D Gilchrist[1,*]

[1] *Department of Mechanical Engineering, University College Dublin, Belfield, Dublin 4, Ireland*

[*] *Corresponding author: Michael.Gilchrist@ucd.ie*

Abstract: In order to create a useful computational tool that will aid in the understanding and perhaps prevention of head injury, it is important to know the quantitative influence of the constitutive properties, geometry and model formulations of the intracranial contents upon the mechanics of a head impact event. The University College Dublin Brain Trauma Model (UCDBTM) [1] has been refined and validated against a series of cadaver tests and the influence of different model formulations has been investigated. In total six different model configurations were constructed: (i) the baseline model, (ii) a refined baseline model which explicitly differentiates between grey and white neural tissue, (iii) a model with three elements through the thickness of the cerebrospinal fluid (CSF) layer, (iv) a model simulating a sliding boundary, (v) a projection mesh model (which also distinguishes between neural tissue) and (vi) a morphed model. These models have been compared against cadaver tests of Trosseille [2] and of Hardy [3]. The results indicate that, despite the fundamental differences between these six model formulations, the comparisons with the experimentally measured pressures and relative displacements were largely consistent and in good agreement. These results may prove useful for those attempting to model real life accident scenarios, especially when the time to construct a patient specific model using traditional mesh generation approaches is taken into account.

Key words: Head impact biomechanics, finite element modelling.

INTRODUCTION

Traumatic head impact injuries occur when the human skull and brain are rapidly subjected to intolerable levels of energy. There exist many causes of neurotrauma; accidents, falls, assaults and injuries occurring during occupational, recreational and sporting activities. The relative ratio of these causes differ worldwide. While RTAs (road traffic accidents) tend to be the leading cause of injury related death, falls tend to be the leading cause of non-fatal hospitalisation [4, 5]. In Ireland, falls are the single greatest cause of hospital admissions for both males and females across most age groups, with head injuries occurring in approximately a quarter of all fall admissions [5]. In the United States, traumatic brain injury results in over 50 thousand fatalities and nearly one million injuries each year. Motor-vehicle crashes are the most common cause of brain injury. Since the introduction of automotive restraint systems such as airbags used in conjunction with seat belts, many forms of injury have been reduced, including brain injury. However, it has not been eliminated as an automotive-related injury and head injuries continue to be sustained by cyclists, pedestrians and motorcyclists.

Much of what is known about brain injury mechanisms in living humans has been as a result of experimental studies. Tests have included physical models, human cadavers and both anaesthetised and cadaveric animals. Experiments conducted on living humans have defined the response of the head to non-injurious impact [6]. Human cadaver experiments have the advantage of accurate anatomy, but the limitation of not properly representing the physiology of the living human (although attempts have been made to simulate vascular lesions by pressurising the vascular system prior to impacting cadaver heads). On the other hand the anaesthetised animal is a living subject but differs anatomically from the human. Highly

Corresponding Author:
Prof. Michael D. Gilchrist, Department of Mechanical Engineering, University College Dublin, Belfield, Dublin 4, Ireland
Tel: +353-1-7161890 Fax: +353-1-2830534
Email: michael.gilchrist@ucd.ie

sophisticated experimental techniques have been developed in the course of animal-based head injury studies. Although the anatomical differences are least in the non-human primate, the smaller size of the monkey skull and brain introduce problems of dimensional scaling when attempting to relate associated results to the living human. Experiments have been conducted on physical models of the brain and have included measurements of strain. These were recorded by measuring the distortion of an impregnated grid or by using photoelastic techniques, in accelerated gel-filled containers (eg. [7, 8]).

Ward and Thompson [9] suggested that the relative motion between the brain and skull could explain many types of brain injury such as intracerebral haematomas, which are principally due to rupture of bridging veins. Since the skull and brain are of different densities and the cerebrospinal fluid (CSF) surrounds the brain, the brain can move relative to the skull during a blunt impact event causing contusions, intracerebral bruises and contrecoup lesions [10]. Bandak [11] categorized this type of "Relative Motion Brain Injury" as a class of focal injuries caused by the tangential motion of the brain relative to the skull, resulting in some classes of focal contusions or blood vessel rupture.

Brain movement within an externally loaded skull poses a complex three-dimensional dynamic boundary value problem. With the rapid advances in computer technology, sophisticated computer models of the head can provide useful information in the investigation of neurotrauma due to impact. The internal biomechanical responses of the brain cannot be completely measured by experimental techniques without introducing large complexity and/or cost, and so finite element (FE) models may be used to study impact events. Moreover, they reduce the need to conduct a large number of experimental tests. In particular, a FE model that describes in detail the complex geometry and the multiple material compositions of the brain can be used to calculate internal stress, strain and pressure at all locations and at any given instant during an impact [12]. Results from such a model can be used to relate the severity and extent of pathophysiological changes and/or structural failure to the magnitudes and directions of input mechanical variables. These models, if validated rigorously, can be used to design countermeasures to mitigate brain injuries in the future.

Only 3D FE models of the human head are suitable for simulating most impact and inertial load analyses. Due to the low shear resistance and large bulk modulus of the intracranial contents, material exchange between regions is likely to occur (CSF, foramen magnum etc.), when the head is subjected to large deformations. This can only be described using 3D models [13]. However, 2D models are useful for parametric studies of controlled planar motions. Also, 2D models simplify the inclusion of geometrical details compared to a corresponding 3D model (for example [14, 15]). Many attempts have been made over the past thirty years to model the human head in three dimensions by finite element analysis. Shugar [16] developed a 3D model of the skull in 1975 and described its method of construction and limitations. Hosey and Liu [17] constructed a model which included all the main anatomical features of the head, albeit in a coarse mesh. The model was subjected to a sagittal impact and it was found that pressure varied linearly across the model, with positive pressure at the coup side, and negative pressure at the contre-coup, with a point of zero pressure over the anterior of the foramen magnum. Ward [18] constructed a physically accurate brain model which included the membranes and the CSF. The skull was not included and instead was modeled by a boundary condition. Major findings were that the internal folds of the dura influenced the response and he postulated that high normal stresses cause serious brain injury, and that combined tension and shear stresses produce subarachnoid haemorrhage. Ruan [19] constructed a detailed 3D model of the head which is still being used a decade later. The model was subjected to frontal, side, and occipital impacts. He found that viscoelasticity had no significance on the pressure response in short duration frontal impacts, and that impactor velocity had more effect than impactor mass. DiMasi [20] created a model which included a skull and brain with simplified shape. That work concluded that there exists higher shear strain for windshield impact compared with A-pillar impact. Khalil and Viano [21] and Voo et al., [22] have reviewed these older models. More recently, Claessens [23] constructed a model and used it for parametric tests. Zhou [24] showed that differentiation between gray and white matter and inclusion of the ventricles (the regions were constructed manually slice by slice in his model) are necessary to match regions of high shear stress to locations of DAI. This model was later updated and further tested by Al-Bsharat [25]. Kang et al. [26] constructed a 3D model of the head and validated it against the three cadaver tests of Nahum [33], Trosseille [2] and Yoganandan [27] and included a fracture criterion in their model. This model was further tested against motorcycle accident cases. These and some others have been reviewed by Kleiven [13] who constructed a 3D model and related injury to both brain and head size. Zhang et al. [12] at Wayne State University have constructed what is currently the highest density mesh which also has a detailed facial structure. Of all the aforementioned models, only those of Al-Bsharat [25], Kleiven [13] and Zhang [12] have been compared to the relative displacement data of Hardy [3].

With regard to the particular methods used to construct the various finite element models, Bandak [29] and Krabbel et al. [30] developed procedures for generating a detailed FE model of the human skull from CT scan images. Both suffered somewhat with problems in creating a well-conditioned element mesh. Kumaresan et al. [31] used the upper limits of the landmark coordinates of the external geometry of a dummy head and divided the head into 33 layers in the horizontal plane. Horgan and Gilchrist [1] showed a number of sections through the contours of the

 doi:10.1533/ijcr.2004.0299

intracranial space and suggested how these may be used to create other FE models of the head.

The present authors have recently constructed [1] a new 3D FE representation of the human head complex, shown in Figure 1, using anatomical data from [32]. The model contains both shell and solid elements, all of which are hexahedral and not tetrahedral. When constructing the model, emphasis was placed on element quality and ease of mesh generation, as this has proved to be a difficulty in other models. The model was validated against the pressure response of Nahum's [33] cadaveric impact test. A parametric study was also performed on the material properties of the intracranial contents for the same cadaver test. It was found that the short-term shear modulus of the brain and the bulk modulus of the CSF had the greatest effect on the pressure response. The effect of skull topology, CSF depth and overall model weight were also investigated and it was found that careful consideration of each is required when attempting to predict the intracranial pressure response.

Clearly, significant effort in using 3D FE models to simulate head impact injury has taken place in the past three decades. None of these models represent the true physiological and anatomical details of the head. All involve various simplifying assumptions concerning geometry, boundary and loading conditions, constitutive properties and element formulations. For example, should linear or higher order shell or solid elements be used, is it necessary to consider the influence of the scalp, face or pia in predicting the occurrence of an injury, or how can the CSF be modelled most simply? To date, no research effort has attempted to establish the consequences of such widely different levels of simplification. Similarly, no in-depth comparison has yet been made of the predictions obtained by a number of these different models when simulating even the simplest of impact cases. This paper attempts to address this knowledge deficit: variations of the baseline UCDBTM are analysed and the different predictions compared against experimental measurements of intracranial pressure and brain motion. The results of this investigation serve to clarify the degree of complexity required in 3D FE models when simulating brain trauma.

CONSTRUCTION OF THE FE VARIATIONS

Baseline Model

This model has been described in detail elsewhere [1] and is shown in Figure 1. The baseline model includes the cerebrum, cerebellum and brainstem, intracranial membranes (falx and tentorium), pia, cerebrospinal fluid layer (CSF), dura, a varying thickness three-layered skull (cortical and trabecular bone layers), scalp and the facial bone. 7,318 hexahedral elements represent the brain and 2,874 hexahedral elements represent the CSF layer with one element through the thickness.

Sliding Boundary Model

A model was built with a sliding boundary between the pia and the CSF layer. The ABAQUS algorithm allows no separation of the contacting pia and CSF layers and thus prevents the formation of a gap at the CSF–cerebrum interface. Considering the effect of fibrous trabaculae and the fluid nature of the CSF, material properties assumed for the solid elements which were used for the CSF were the bulk modulus of water and a very low shear modulus. For all the sliding interfaces a friction coefficient of 0.2 was used, as proposed by Miller et al. [34]. The CSF which exists between the falx and the brain, and between the tentorium and cerebrum/cerebellum was also included using the same type of fluid–structure contact algorithm.

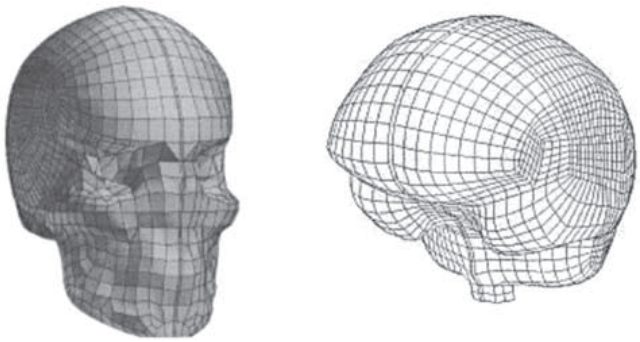

Figure 1 Overview of baseline finite element model (whole head, left; brain, right), i.e., baseline UCDBTM.

Grey-White-Ventricular Matter Model (GWV Model)

The physiological accuracy of the baseline UCDBTM was refined by explicitly distinguishing between grey matter, white matter and the ventricles. Hexahedral meshing along the boundaries of such regions would require an unnecessary mesh development effort and the distinction between these types of neural tissue was conveniently made by modifying the baseline finite element mesh in such a way that elements were assigned material properties appropriate to these corresponding regions of the cerebrum.

In a method similar to that described in [35], the MRI scans of the head were registered with the cerebral elements in space using a purpose-written program created in MATLAB [36]. Each element then performed a global search to find the MRI voxels in its vicinity, and then performed a more detailed local search to discover exactly what elements were contained within its volume. Figure 2 shows how this algorithm operates schematically.

The elements of the FE mesh may not have their facets aligned with the MRI grid axis. It is known from computational geometry that the volume of a tetrahedron, of vertices a, b, c, d can be evaluated directly from the coordinates of its vertices by computing the determinant of the 4×4 matrix:

$$\begin{vmatrix} a_0 & a_1 & a_2 & 1 \\ b_0 & b_1 & b_2 & 1 \\ c_0 & c_1 & c_2 & 1 \\ d_0 & d_1 & d_2 & 1 \end{vmatrix} = 6V \qquad [1]$$

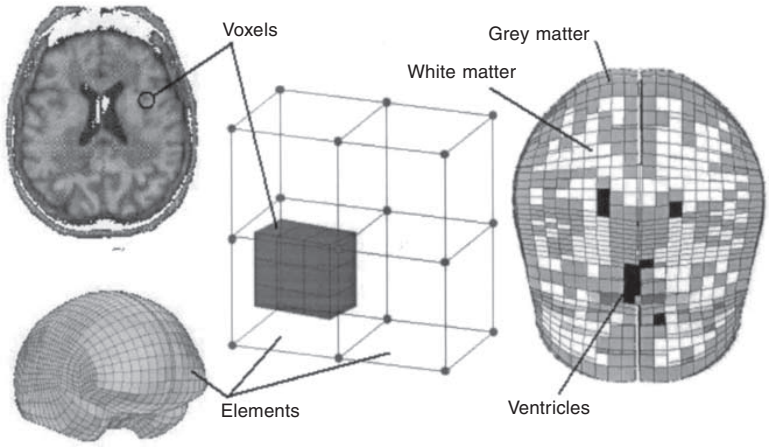

Figure 2 The basis upon which the purpose-written MATLAB program works involves two steps to assign specific material properties to the elements of the cerebrum. The MRI voxels and finite elements within the FE model are registered to occupy the same space. Each element identifies which voxels are contained within its six faces. By an appropriate choice of threshold values of voxel intensities, the element is assigned the constitutive properties for grey, white or ventricular matter, although the MATLAB program can assign intermediate properties to each element uniquely.

This volume, V, has a positive sign if (a, b, c) form a counterclockwise circuit when viewed from the facet opposite d. In other words, the right hand rule would have a thumb pointing away from d if the fingers were turned in the direction of abc, as illustrated in Figure 3.

Any hexahedron element, which is the only type of solid element used in the UCDBTM, can be decomposed into tetrahedrons. If there is a positive volume for each and every tetrahedron formed by the vertices of the triangles formed on the facets of a given hexahedron element and the centroid of a given voxel, then that voxel is fully contained within the hexahedron element. Once it is known which voxels are contained within a given hexahedron element, the intensity of the voxels is averaged. Based on predefined thresholds, the element is then assigned the properties of grey, white or ventricular (CSF) matter as shown in Figure 2.

3-element CSF Model

It was decided to construct a model that represented a layer of fluid between two surfaces different from a sliding or a tied boundary. Instead, a model was developed to consist of three elements through the CSF layer, the outer nodes being tied to the skull and brain. In this way the 'no-slip' condition of fluid mechanics could be met. Because of the small size of the associated elements, it was decided to use a slightly deeper fluid element model which was developed previously [1]. It was also necessary to use an adaptive meshing algorithm for the CSF layer instead of a purely Lagrangian FE approach so as to maintain element quality. In this formulation, the CSF layer was continually smoothed during the impact simulations, moving the nodes to maintain element quality while mapping the solution from the old mesh positions to the new optimised ones. Figure 4 shows a close up of a cutaway section of the 3-element CSF model near the tentorium. This type of analysis was proposed by Van Hoof et al., [37], who also mentioned that the ALE formulation could be used to more accurately model the foramen magnum.

Problems arose when attempts were made to define an Eulerian boundary condition at the foramen. Namely, every

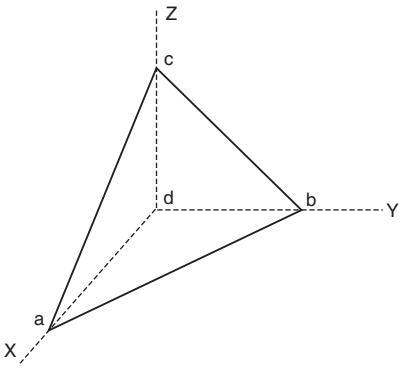

Figure 3 Tetrahedron vertices. The volume of a tetrahedron with vertices at a, b, c and d is positive when calculated using a, b and c in an anti-clockwise fashion.

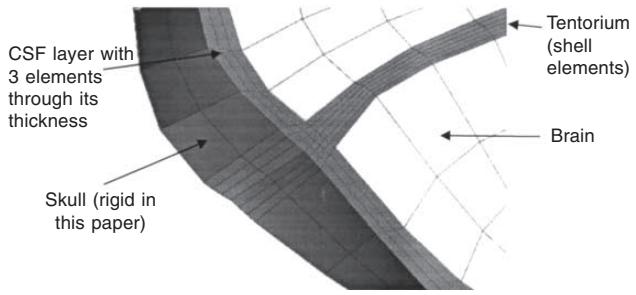

Figure 4 Detail of CSF layer when three elements were placed through the thickness rather than one. The size of the resulting elements between the skull and the intracranial membranes required the use of adaptive meshing.

 doi:10.1533/ijcr.2004.0299

node at the foramen magnum, which is the exit of the system, must have its path defined. This required the definition of a very large number of separate amplitude curves for the ABAQUS input deck. Also, at the time of writing, it was not possible for both the brain stem, and fluid around it, to have an Eulerian exit. As a consequence during the analysis, nodes at the exit were moving in a Lagrangian sense out of the system (nodes and material leaving the system) and in an Eulerian sense (nodes remained planar, while material was leaving the system). Element distortion at the intersection, in the region of the foramen, eventually became too high and the analysis failed.

Projection Mesh Model

If a regular square grid is deformed in such a way as to form a circle (Figure 5), it would produce 4 elements, corresponding to the four corners of the block, which are highly distorted. As the mesh density of the circle is increased, the internal angle of these elements approaches 180 degrees. These and adjacent elements will be ill-conditioned and this is particularly problematic for analyses where the outer regions are of greatest interest and where numerical accuracy is required to be highest. An alternative mesh generation scheme, referred to as the projection mesh method, does not involve this distortion of a square mesh. Instead, as shown in Figure 5(b), the corners of an undistorted square mesh locate the origin of projection lines which radiate outwards to the boundary of a circular shape (spherical in 3D). These projected lines, in turn, define the edges of rows of quadrilateral elements (hexahedral in 3D). Because of the definite change in mesh structure at the boundary of the square, the quality of the elements in the projection region will not degrade further, regardless of how refined the mesh density is made.

This technique of meshing curved objects using multiple blocks is commonly used. The 3D analogue of the circle is the sphere. Figure 5 (c) shows how a single cube lying at the centre of a spherical object can be used to construct a 3D mesh via the projection mesh method. Six more blocks, each extruding from one of the 6 faces of the centre cube complete the sphere [38]. Figure 6 explains a set of rules that can be followed to formalise this process.

Figure 7 compares the element shapes of the projection mesh and baseline models in part of the occipital lobe. The more regularly shaped elements of the projection mesh model are evident throughout the region whilst elements in the baseline model are not as well-conditioned and have high internal angles and aspect ratios close to the outside. Table 1 quantifies the relative percentage of poorly-conditioned elements in each mesh. Fewer elements of poor quality exist in the projection mesh model than in the baseline UCDBTM and these poor elements are away from the brain-skull interface whereas they are closest to this critical interface in the baseline model. In the regions

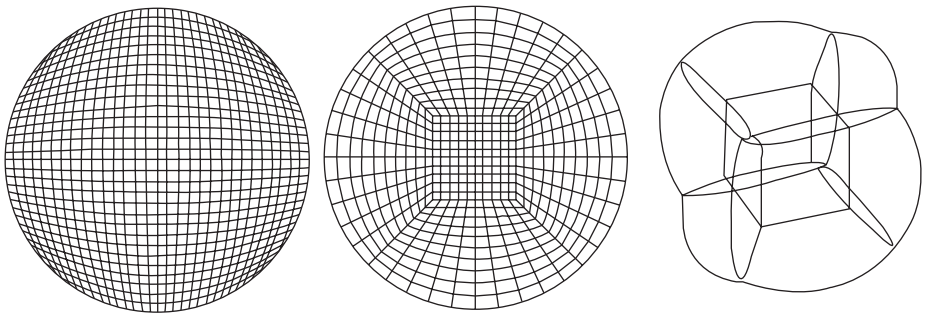

Figure 5 The swept mesh method (a) is simple to implement but will not be numerically well-conditioned if only quadrilateral elements are used. The projection mesh method involves two meshing steps but combines good element quality throughout the resulting mesh with the complete use of quadrilateral (b) and hexahedral elements (c). Images courtesy of the TrueGrid homepage [38].

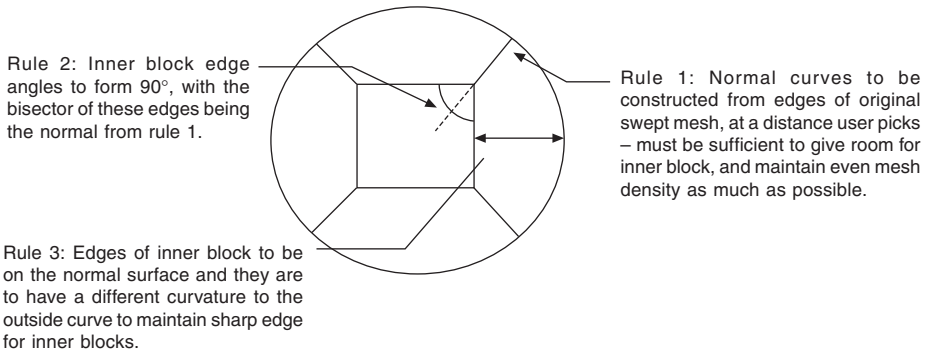

Figure 6 How to change or convert a swept mesh into a projection mesh.

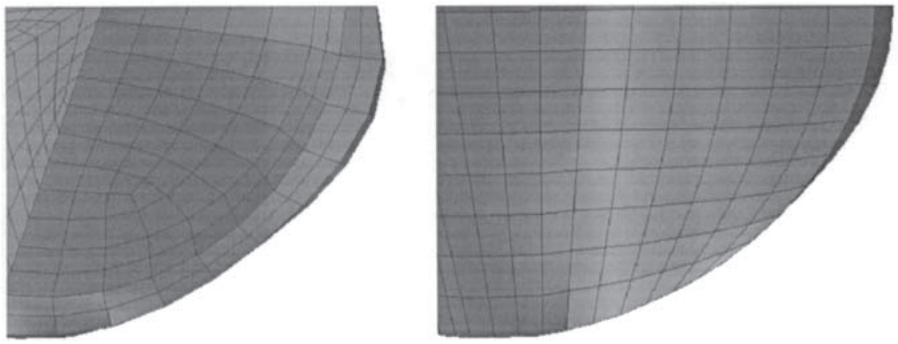

Figure 7 Comparison of element quality in projection mesh model (left) with baseline model (right). Note the large internal angles in the outer elements of the baseline model as compared to those in the projection mesh model.

Table 1 **Comparison of projection mesh model with baseline mesh model in terms of individual hexahedron element quality. Note that for the baseline model, the proportionate increase of high edge angled elements would increase with increasing mesh density**

Projection Mesh Model	Baseline Mesh Model
No. Elements (Brain) : 12,776	No. Elements (Brain) : 7,318
No. Elements with internal angle > 150° : 186	No. Elements with internal angle > 150° : 367
Percentage: 1.4%	Percentage : 5%

of the brain stem and where the midbrain transitions to the temporal lobe, further methods (not reported here) were used to update and improve the element quality while retaining the ability for the user to choose the refinement level.

A further advantage of the projection mesh model is that its element density can be increased to any desired level without loss of element quality; a corresponding increase in element density of the baseline model would reduce the mesh quality at the outer sides of the brain. The implications for future modelling activity is that the very large mesh densities that are required to properly simulate the propagation of compressive waves of ballistic impacts using explicit finite element solvers (elements of order 50 μm in size [39]) will most likely be developed via projection mesh methods. Longer duration impact events (falls, pedestrian and RTAs) do not require meshes of such high element density.

Morphed model

It was of interest to see how the pressure and displacements of the FE model would change if a different intracranial space (other than that of the visible male's) was modelled. Creation of another entire head FE model, even with knowledge of where the decomposition sections should be [1], was deemed outside the scope of this work. Instead the feasibility of morphing our existing model to that of another head to some degree was investigated. The method of the thin plate splines was employed. This has the basis that a plate with isotropic properties (eg. Steel) can be morphed to fit a homologous shape (a shape that can be formed from the original without joining, crossing or tearing the original shape) by means of applying forces and constraints to 'bend' the plate to the new desired shape. Instead of writing a program to perform this morphing, a combination of the Patran [40] and ABAQUS [41] software was used instead to force the model into reshaping.

A coarse mesh was constructed on the baseline model (Figure 8(a) and (b)) and this was then warped (simple scaling in the X, Y and Z domains) to fit the global x, y and z dimensions of a new skull [42]. Vectors were constructed by picking points on the coarse grid and their matching landmark point on the new skull (visually, Figure 8(c)), until every point on the coarse grid had a displacement vector associated with it. A static displacement analysis, using all of these displacement vectors as input, was then carried out on this coarse grid (giving it isotropic

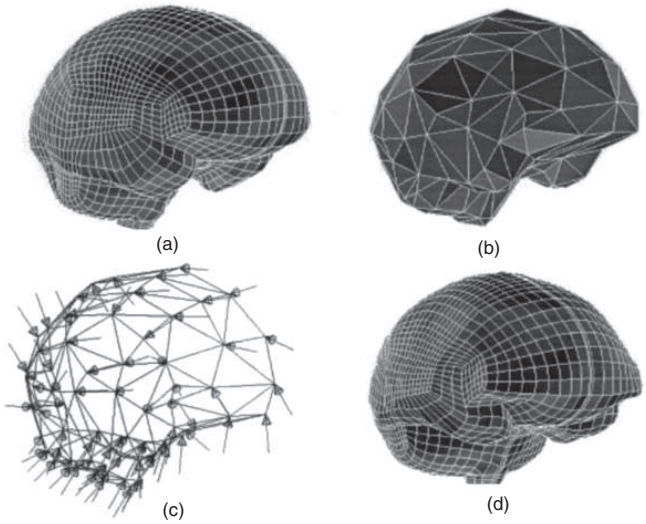

Figure 8 Steps used to make the morphed model. A coarse grid (b) was constructed on the original model (a). A discrete field of displacement vectors was then applied to every node of this coarse grid (half of which are visible in (c)), and this field was converted into a continuous field in order to create (d). The morphed model is of Van Lierde and Vander Sloten [42] while the original model is of the visible male [32].

 doi:10.1533/ijcr.2004.0299

properties) and the results were read into MSC/Patran [40]. Patran was then capable of converting the resultant vector plot into a continuous spatial displacement field. This new continuous displacement field was then applied to the projection mesh model at the dura and a new static displacement analysis was carried out on the entire projection mesh model (again giving all elements identical isotropic properties). This then forced the intracranial shape to move from its original state to match that of the new intracranial shape. Finally these new analysis results were read into Patran once again and another utility was invoked to move the original nodal positions, strain free, to those of the deformed positions (Figure 8(d)).

Constitutive property assignment

The baseline model was previously validated against the pressure information of the cadaver test of Nahum and has been discussed previously [1]. It was noted before that changes in intracranial properties affected different simulation results using this model by different amounts. The material properties used in this present paper are presented in Table 2. Models which do not have the cerebrum sectioned into different materials use the same material properties as in our earlier publication (those of Mendis [43]), and those that are differentiated use the softer properties that are currently being used by Wayne State University [12], which were chosen for comparison and because they are the latest available properties for these regions.

SIMULATION RESULTS

Predictions of intracranial pressure during impact

The baseline and five variant FE models were used to simulate Trosseille's cadaver impact test [2]. The mechanics of this experiment were more complicated than the cadaver test of Nahum [33], which had been used previously to validate the baseline model [1]. Unlike Nahum's test, where the line of action of the impact passed through the center of mass of the cadaver head, Trosseille's test involved both rotational and translational acceleration components. This experiment was designed to replicate head impact against the steering wheel of a car. The cadavers were unembalmed and the brain was re-pressurised. A 12-accelerometer array was screwed into the skull in the occipital region to measure the entire 3D kinematics of the head. Miniature pressure transducers were placed in the subarachnoid space and in the ventricular system to measure intracranial and ventricular pressures. The cadavers were suspended in a sitting position and were impacted by a 23.4 kg impactor at a velocity of 7 m/s in the antero-posterior direction, in the facial region. For the present simulation, experimental results from Test No. MS 428_2 [44] were made available. These data included histories of the three translational and three rotational acceleration components at the center of gravity (CG) of the head, intracranial pressures measured in the frontal and occipital lobes, and ventricular pressures in the lateral and third ventricles. This impact situation was conveniently simulated with the present finite element models by applying the six time varying components of the linear and angular velocity measured experimentally to the FE models (up to 35 ms of the recorded data). The predicted intracranial pressures in the frontal and occipital regions as well as the ventricular pressures in the lateral and third ventricles predicted by the model were compared with those obtained experimentally to validate the model.

Figures 9 and 10 compare the experimental and simulated frontal and occipital pressures while Figure 11 compares the pressure at the lateral ventricle (baseline and GWV models only). General shape trends and duration of the pressure pulses agree while the magnitudes differ, especially in the case of the occipital lobe. In some analyses there exists an initial oscillation before the maximum pressure is reached. The reason for this is due to slight differences in shapes of the models, the longer and flatter models producing more of this initial peak, especially in the case of the morphed model. Apart from the sliding

Table 2 **Material properties used in the analyses. For some analyses the CSF layer required a small value for stiffness in shear in order for the test to run to completion**

	Density	Shear Modulus (kPa)		Decay constant	Bulk Modulus
	(kg/m^3)	G_0	G_∞	(s^{-1})	(GPa)
Grey matter	1060	10	2	80	2.19
White matter	1060	12.5	2.5	80	2.19
Brainstem	1060	22.5	4.5	80	2.19
Cerebellum	1060	10	2	80	2.19
Baseline model	1040	Hyperelastic [43]			2.19
Falx, Tentorium,	Density	Elastic Modulus		Poisson's Ratio	
Dura	1140	3.15E+7		0.45	
Pia	1130	1.15E+7		0.45	
CSF	1000	Water		0.5	

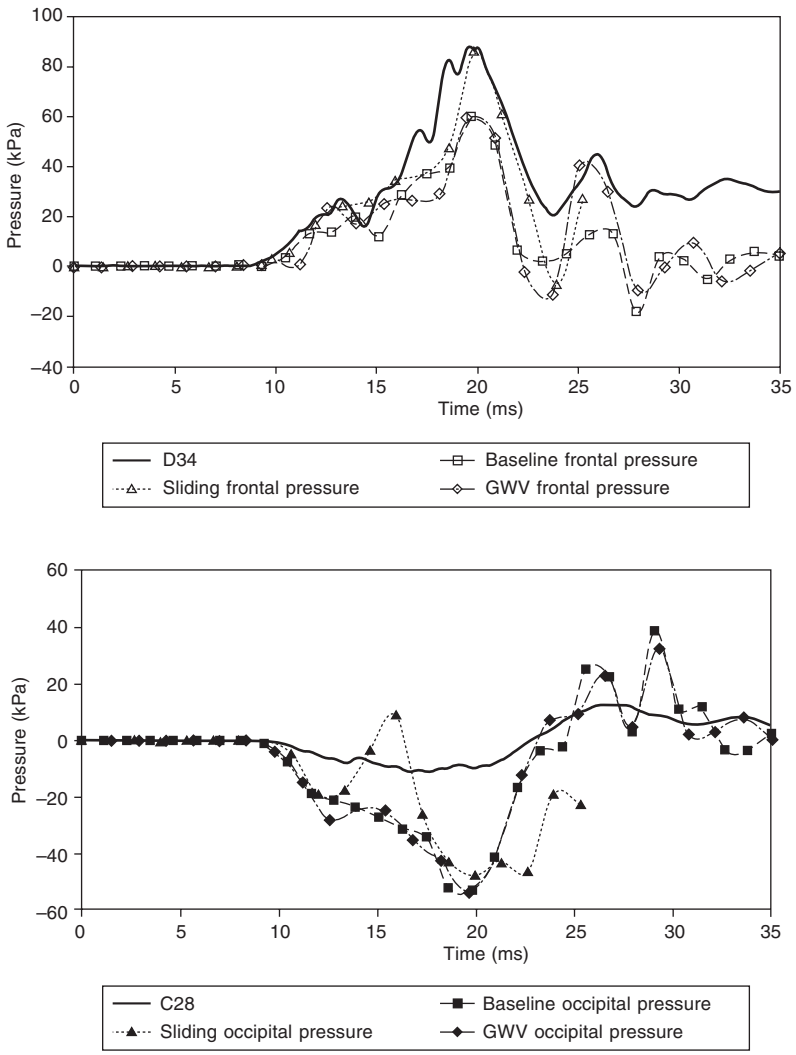

Figure 9 Experimentally measured [2] and simulated predictions of frontal pressure. D34 and C28 represent the names of the experimental frontal and occipital pressure responses, respectively.

boundary model, all remaining models underestimate the frontal pressure, and overestimate the occipital pressure. This trend, was not observed in the earlier comparison against the simpler cadaver experiment of Nahum. This behaviour was also noted by Willinger et al [45]. The sliding model exhibits a similar frontal pressure, but this is most likely due to the contact formulation in this area. All models demonstrate similar pressure responses; with only some effect being noticed for different fluid layer constructions – the 3 element CSF model and the sliding boundary model having somewhat higher frontal pressure traces. Some difference is also seen for the morphed model. This is believed to be mainly due to the longitudinal axis of the head – the morphed model being slightly 'flatter' than the baseline model. Even when comparing the pressure at the lateral ventricle, the baseline model and the GWV model (the properties of which are different in this region) predict quite similar values.

Predictions of brain displacement during impact

Experimental data from recent cadaver head impact experiments of Hardy and Kleiven provided vectorised information on the motion of different regions of the brain during impact [3, 46]. In Hardy's experiment, two sets of neutral density targets with approximately the same density as brain were inserted in two vertical columns into the brain. The cadaver head was impacted and the positions of the targets were tracked during the impact event. These position vectors were then converted into a moving coordinate system so as to determine the relative displacement of the targets with respect to the skull. In order to compare the predictions of the UCDBTM against this displacement data, the six experimentally measured velocity components were applied to the CG of the model. The assumption of a rigid skull was necessary in order to satisfy the rigid body criteria used to obtain the six acceleration components. By assuming that the CG of the FE model was coincident with that of the cadaver head, the kinematics of the FE head would be exactly the same as those of the cadaver head for any given impact [12]. The displacements were measured in a coordinate system fixed to the head as shown in Figure 12, which shows the

 doi:10.1533/ijcr.2004.0299

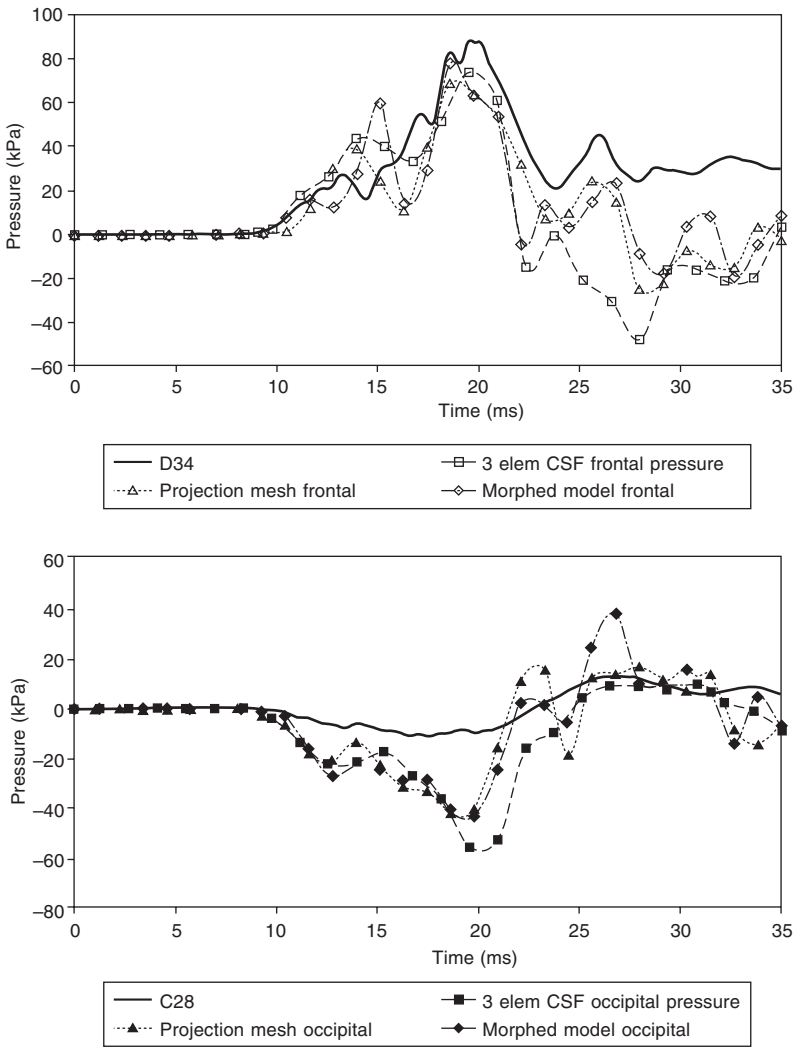

Figure 10 Comparison of remaining 3 models' pressure response versus the Trosseille experimental data.

comparison between the experimental relative displacements (projected onto the X-Z plane) and those predicted numerically by the UCDBTM. For ease of viewing, results in Figure 12 show only the results of the GWV model. This model had slightly more brain motion and more accurately reproduced the experimental traces than the baseline model, in particular for those of the superior markers 5, 6, 11 and 12. Figures 13, 15 and 16 show the displacements predicted by the GWV model in greater detail. Note that in the relative X and Z displacement plots of Figure 13, the starting positions were not exactly coincident, but were adjacent.

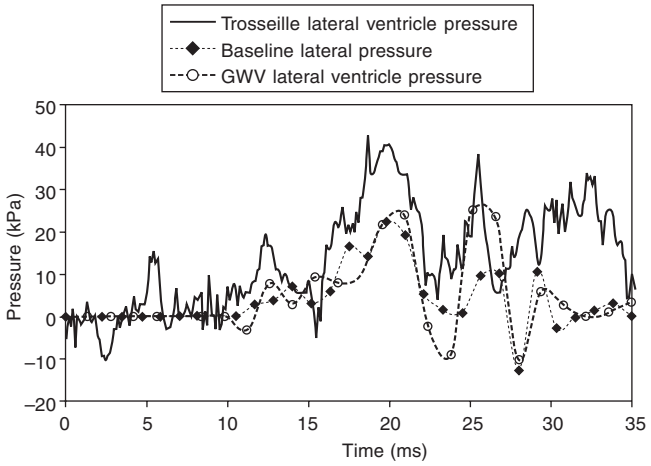

Figure 11 Comparison of experimental and simulated pressures at the lateral ventricle for the baseline and the GWV model. Pressure is measured at the same element for both models.

Figure 14 shows a relative displacement fringe plot indicating the amount of movement taking place in the brain relative to the moving skull. The outside of the cerebrum moves a very small amount while the core of the brain has the dominant relative motion. The remaining plots for the other 5 models are in the Appendix. Results for every model were very similar with the displacement traces sitting almost on top of each other.

CONCLUSIONS

The baseline UCDBTM has previously been validated

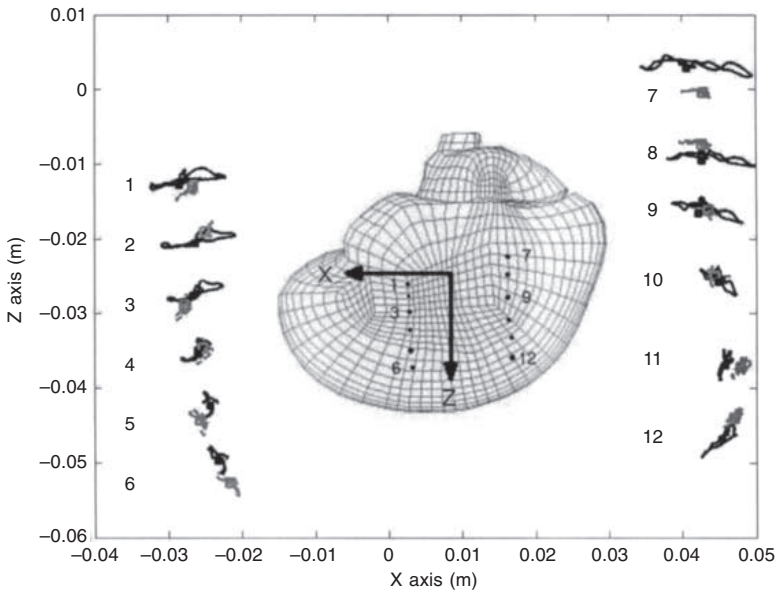

Figure 12 Overview of results comparing predicted and measured brain displacements (relative to the skull). The black curves represent the experimental trace of brain motion, while the grey curves show the simulated results. The direction of motion is qualitatively predicted and, in the case of the superior markers, accurate magnitudes of direction are also predicted.

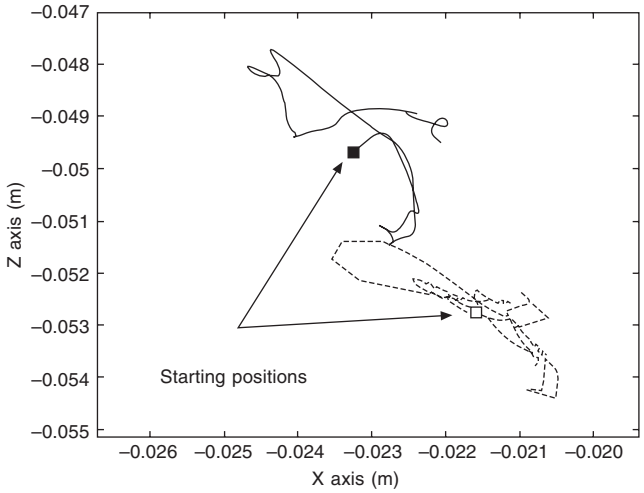

Figure 13 Close up on path taken by NDT 6 in experiment (solid line) and path taken by the closest equivalent node in the simulation (dashed line). The solid black box indicates the starting position for the experimental data while the open black box is the initial position of the adjacent node.

against the pressure data of Nahum. In that paper [1] tests were also carried out on the model's response using different intracranial properties and element formulations for the skull. It was seen that quite large changes in material properties could effect noticeable changes in the pressure response but larger differences in the Von-Mises response. Six different variations of the UCD Brain Trauma Model were constructed and their method of construction is reported in this paper. These were: (i) the baseline model, (ii) a model simulating a sliding boundary, (iii) a refined baseline model which explicitly differentiates between grey and white neural tissue, (iv) a model with three elements through the thickness of the cerebrospinal fluid (CSF) layer, (v) a projection mesh model (which also distinguishes between neural tissue) and (vi) a morphed model. These six variant models were compared against two cadaveric tests: one to measure the variation of intracranial pressure during impact and the second to measure the motion of the brain relative to the skull during impact. The following conclusions can be drawn:

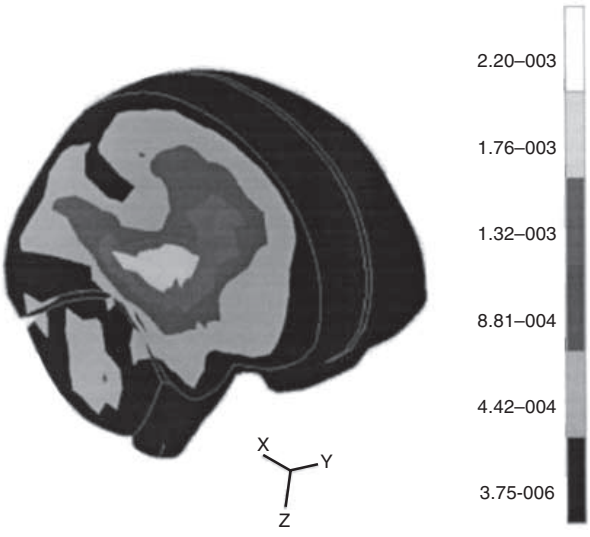

Figure 14 Still from GWV model at 26 ms during Hardy impact simulation (time chosen to match that of the first peak motion seen in the experimental motion shown in Figure 15). Image shows a fringe plot of the relative displacements (in metres) of brain elements with respect to the skull. The greatest relative motion is towards the interior of the cerebrum, while the outside region moves essentially in unison with the skull.

 doi:10.1533/ijcr.2004.0299

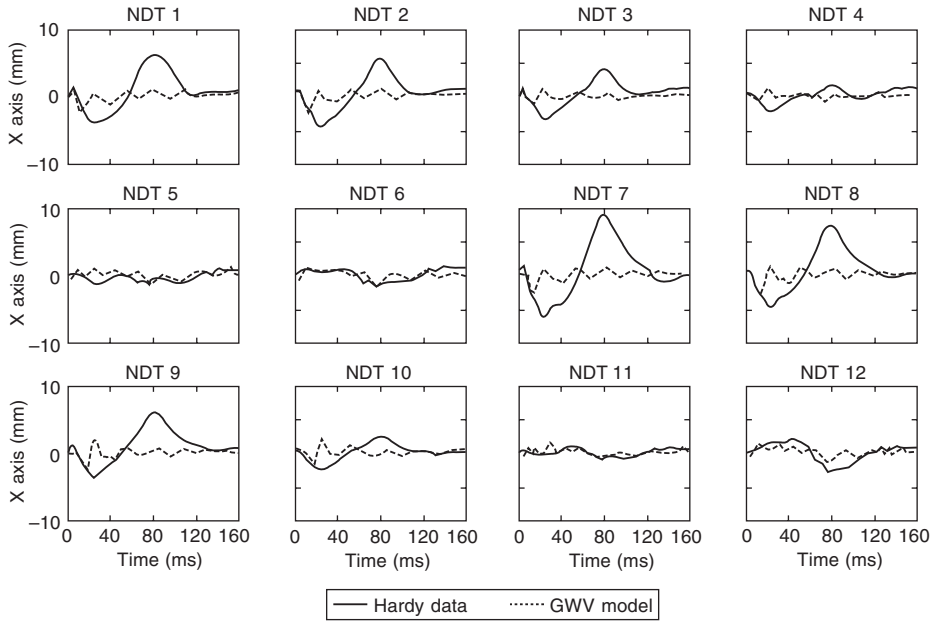

Figure 15 Comparison of the simulated relative displacements against the data of Hardy et. al. [3] for the GWV model. Displacements here are in the local X direction. The accuracy of the more inferior markers (1-4, 7-10) is poorer than those of the superior markers (5, 6, 11 and 12), where more simulated brain motion takes place.

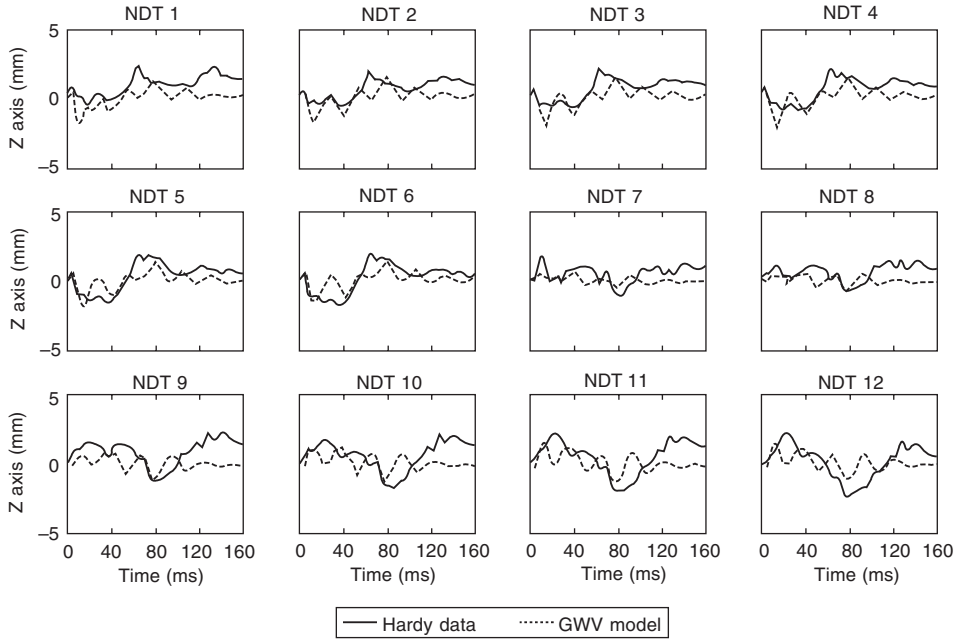

Figure 16 Comparison of the simulated relative displacements against the data of Hardy et. al. [3] for the GWV model. Displacements here are in the local Z direction. The impact direction being in the Frankfort x-direction, the magnitudes of motion in the z direction are smaller than in the x.

- All six models were compared against test MS428-2 of Trosseille's cadaveric test, where the variation of intracranial pressure during impact was recorded. Little evident difference was noted when the models were compared against the intracranial pressure. Even in the case where the finite element model distinguishes between the grey, white and ventricular matter the results were consistently similar. The most notable difference was observed when comparing the sliding boundary model's pressure response, though this is more likely to be due to the penalty contact formulation used. Some difference was noticed in the case of the morphed model. Whether this was more due to the major and minor axes of the head (anterior-posterior lengths etc.) or to the subtle differences in shape requires further investigation.
- The six models were also compared against test C383-T4 of Hardy et al.'s cadaveric test, where the variation

of the motion of the brain relative to the skull during impact was measured. Again little evident difference was noted when the models were compared against the relative motion data. This would seem to indicate that the advancements on the baseline model may not have improved its prediction capabilities, and as a corollary, a model with the attributes of the baseline model may suffice when modelling brain injury.

In the case of the models which distinguish between different types of neural tissue, it is likely that more elements would be required to gain full advantage of the automated material reassignment program. Alternatively, a simpler representation of the ventricles, which could have more clearly defined meshed boundaries with the neural tissue, would present more of a useful improvement. That system may give further insight about stress distribution around the horns of the ventricles under impact and the subsequent likelihood of diffuse axonal injury, such as presented in [15]. Also, further information may be gained as to the models' relative differences if softer material properties were used as suggested and implemented in [47], as any differences between models too small to see here, would become magnified (equivalent initial Young's modulus for the hyperelastic model would be similar to that of the GWV models' for this paper).

The brain motion data of Hardy is the most recent and most advanced cadaver data against which computational models can be compared. Various hypotheses exist for the mechanisms of brain injury including strain [47, 48], strain rate [49], Von-Mises stress [44, 50] and the product of strain and strain rate [51]. Predictive finite element models must give greater emphasis to accurately predicting other engineering values as well as pressure (e.g., relative skull/brain motion).

ACKNOWLEDGEMENTS

The authors wish to acknowledge the data provided by Svein Kleiven, Xavier Trosseille and Warren Hardy, and the additional discussions with David Viano and Daniel Baumgartner. The assistance of Michael Conry, Amir Tabakovic and Mary Doorly is also appreciated. This work was funded by Enterprise Ireland and the PRTLI – National Neuroscience Network.

Obtaining a copy of the UCDBTM

Interested readers can obtain a copy of the baseline UCDBTM at no cost to download using the method described at the BEL mesh repository website:
http://www.tecno.ior.it/VRLAB/researchers/repository/BEL repository.html#head
It is usable under the BEL license agreement.

REFERENCES

1. Horgan, T J and Gilchrist, M D. 'The creation of three-dimensional finite element models for simulating head impact biomechanics', *International Journal of Crashworthiness*, 2003 **8** (4) 353–366.
2. Trosseille, X, Tarriere, C, Lavaste, F, Guillon, F and Domont, A. 'Development of a F.E.M. of the human head according to a specific test protocol', Proc. 36th *Stapp Car Crash Conference,* SAE Paper No. 922527, Society of Automotive Engineers, Warrendale, PA, 1992.
3. Hardy, W N, Foster, C D, Mason, M J, Yang, K H and King, A I. 'Investigation of head injury mechanisms using Neutral Density Technology and high-speed biplanar X-ray', *Stapp Car Crash Journal*, 2001 45 337–368.
4. Watson, W L and Ozanne-Smith, J. 'Injury surveillance in Victoria, Australia: Developing comprehensive injury incidence estimates', *Accident Analysis and Prevention*, 2000 **32** 277–286.
5. Scallan, E, Staines, A, Fitzpatrick, P, Laffoy, M and Kelly, A. 'Injury in Ireland. Report of the Department of Public Health Medicine and Epidemiology', University College Dublin, 2001.
6. McLean, A J and Anderson, R W G. 'National Neurotrauma Society Guest Book, Part One: The Injury, Chapter 2: Biomechanics of closed head injury', 25–37 http://www.edc.gsph.pitt.edu/neurotrauma/thebook/book.html
7. Margulies, S S, Thibault, L E and Gennarelli, T A. 'A study of scaling and head injury criteria using physical model experiments', Proc. *IRCOBI/AAAM Conf.*, Göteborg, 1985 223–235.
8. Holbourn, A H S. 'Mechanics of head injuries', Lancet, 1943 ii 438–444.
9. Ward, C and Thompson, R. 'The development of a detailed finite element brain model', Proc. 19th *Stapp Car Crash Conference,* SAE Paper No. 751163, 1975.
10. Gurdjian, E and Gurdjian, E S. 'Acute head injuries', *Surgery*, 1978 **146** 805–820.
11. Bandak, F A. 'Biomechanics of impact traumatic brain injury. Crashworthiness of Transportation System: Structural Impact and occupant Protection', NATO ASI Series, Ambrosio J A C et al. Eds. Kluwer Academic Publishers, The Netherlands, 1997 53–93.
12. Zhang, L, Yang, K H, Dwarampudi, R, Omori, K, Li, T, Chang, K, Hardy, W N, Khalil, T B and King, A I. 'Recent advances in brain injury research: A new human head model development and validation', *Stapp Car Crash Journal*, 2001 **45** 369–393.
13. Kleiven, S. 'Finite Element Modeling of the Human Head', Doctoral Thesis. Technical Report 2002-9, Department of Aeronautics, Royal Institute of Technology, Stockholm, Sweden, 2002.
14. Gilchrist, M D, O'Donoghue, D and Horgan, T J. 'A two dimensional analysis of the biomechanics of frontal and occipital head impact injuries', *International Journal of Crashworthiness*, 2001 **6** (2) 253–262.
15. Nishimoto, T and Murakami, S. 'Direct impact simulations of diffuse axonal injury by axial head model', *JSAE Review* 2000 **21** 117–123.
16. Shugar, L. 'A Finite element head injury model', DOT HS 803-211, NTIS, 1977.
17. Hosey, R R and Liu, Y K. 'A homeomorphic finite element model of the human head and neck', In *Finite Elements in Biomechanics*, Simon, B R, Gallagher, R H, Johnson, P C, Gross, J F (Eds), Wiley and Son, 1981 379–401.

18. WARD, C C. 'Finite element models of the head and their use in brain injury research'. Proc. 26th *Stapp Car Crash Conference*, Society of Automotive Engineers, Ann Arbor, Michigan, 1982 71–85.
19. RUAN, J S. 'Impact Biomechanics of Head Injury by Mathematical Modelling', Ph.D. Thesis, Wayne State University, 1994.
20. DIMASI, F, MARCUS, J and EPPINGER, R. '3-D anatomic brain model for relating cortical strains to automobile crash loading', Proc. *13th Int. Techn. Conf. on Experimental Safety Vehicles*, November 4–7 1991b, Paper no. 91-S8-O11.
21. KHALIL, T B and VIANO, D C. 'Critical issues in finite element modeling of head impact', 26th *Stapp Car Crash Conference*, 1982 87–102.
22. VOO, L, KUMARESAN, S, PINTAR, F A, YOGANANDAN, N and SANCES, A. Jr., 'Finite element models of the human head', *Medical & Biological Engineering & Computing*, 1996 **34** 375–381.
23. CLAESSENS, M. et al., 'Modeling of the Human Head Under Impact Conditions: A parametric Study', 41st *Stapp Car Crash Conference*, SAE Paper No. 973338, Society of Automotive Engineers, 1997 315–328.
24. ZHOU, C. 'Finite element modelling of impact response of an inhomogenous brain', PhD Thesis, Wayne State University, 1995.
25. AL-BSHARAT, A S, HARDY, W N, YANG, K H, KHALIL, T, TASHMAN, S and KING, A I. 'Brain/skull relative displacement magnitude due to blunt head impact: New experimental data and model', *Stapp Car Crash Journal*, 1999 **43** 321–332.
26. KANG, H, WILLINGER, R and DIAW, B M. 'Validation of a 3D Anatomic Human Head Model and Replication of Head Impact in Motorcycle Accident by Finite Element Modeling', Proceedings of the 41st *Stapp Car Crash Conference*, 1997.
27. YOGANANDAN, N, PINTAR, F A, SANCES, A, Jr., WALSH, P R, EWING, C L, THOMAS, D J and SNYDER, R G. 'Biomechanics of skull fracture', In *Traumatic Brain Injury: Bioscience and Mechanics*, Bandak, F A, Eppinger, R H, Ommaya, A K (Eds), Mary Ann Liebert Inc., 1996 227–236.
28. BANDAK, F A and EPPINGER, R H. 'A three-dimensional FE analysis of the human brain under combined rotational and translational accelerations', In 38th *Stapp Car Crash Conference*, Society of Automotive Engineers, 1994 145–163.
29. KRABBEL, G, NITSCHE, S and APPEL, H. 'Development of an Anatomic 3-D Finite Element Model of the Human Head for Occupant Simulation'. Automobile in harmony with human society: 25th Fisita Congress, 1994 82–97.
30. KUMARESAN, S, RADHAKRISHNAN, S and GANESAN, N. 'Generation of geometry of closed human head and discretisation for finite element analysis', *Medical and Biological Engineering and Computing,* 1995 349–353.
31. U.S. National Library of Medicine, National Institutes of Health (NIH), Department of Health & Human Services,Visible Human Database. http://www.nlm.nih.gov/research/visible/visible human.htm
32. NAHUM, A M, SMITH, R W and WARD, C C. 'Intracranial pressure dynamics during head impact', Proc. of the 21st *Stapp Car Crash Conference*, SAE paper no. 770922, 1977.
33. MILLER, R T, MARGULIES, S S, LEONI, M, NONAKA, M, CHEN, X H, SMITH, D H and MEANEY, D F. 'Finite element modeling approaches for pedicting injury in an experimental model of severe diffuse axonal injury', In 42nd *Stapp Car Crash Conference*, SAE Paper No. 983154, Society of Automotive Engineers, 1998 155–166.
34. ZANNONI, C, MANTAVANI, R and VICECONTI, M. 'Material properties assignment to finite element models of bone structures: a new method', *Medical Engineering & Physics*, 1998 **20** 735–740.
35. MATLAB 6.1, MATHWORKS, 2002.
36. VAN HOOF, J, WORSWICK, M J, BEUSENBERG, M and SHEWCHENKO, N. 'Effects of skull-brain interface conditions in finite element head models under impact loading', Biomechanics 1, AMERI-PAM '99 1999.
37. TrueGrid website. www.truegrid.com
38. BRANDS, D W A. 'Predicting brain mechanics during closed head impact – numerical and constitutive aspects', PhD Thesis. Technische Universiteit Eindhoven, 2002.
39. Patran r2a. MSC, 2002.
40. ABAQUS version 6.1, HKS, 2003.
41. VAN LIERDE, C and VANDER SLOTEN, J. Personal communication, Skull 70, 2003.
42. MENDIS, K K, STALNAKER, R L and ADVANI, S H. 'A constitutive relationship for large deformation finite element modeling of brain tissue', J. Biomechanical Engineering, 1995 **117** (4) 279–285.
43. TROSSEILLE, X. Personal communication, 2002.
44. WILLINGER, R, BAUMGARTNER, D, CHINN, B and NEALE, M. 'Head tolerance limits derived from numerical replication of real world accidents', Proc. *IRCOBI Conf.*, 2000 209–221.
45. HARDY, W and KLEIVEN, S. Personal communication, 2002.
46. KLEIVEN, S and HARDY, W N. 'Correlation of an FE Model of the Human Head with Experiments on Localized Motion of the Brain – Consequences for Injury Prediction', *46th Stapp Car Crash Journal,* 2002.
47. SHREIBER, D I, BAIN, A C and MEANEY, D F. 'In vivo thresholds for mechanical injury to the blood-brain barrier', In *Stapp Car Crash* Conference SAE paper no. 973335, 1997 277–291.
48. BAIN, A and MEANEY, D. 'Thresholds for electrophysiological impairment to in vivo white matter', In *IRCOBI Conf.,* Sitges, 1999 83–94.
49. GALBRAITH, J, THIBAULT, L and Matteson, D. 'Mechanical and electrical responses of the squid giant axon to simple elongation', *Journal of Biomechanical Engineering*, 1993 **115** 13–22.
50. ANDERSON, R, BROWN, C, BLUMBERGS, P, SCOTT, G, FINNEY, J, JONES, N and MCLEAN, A. 'Mechanisms of axonal injury: an experimental and numerical study of a sheep model of head impact', In *IRCOBI Conf.* Sitges, 1999 107–120.
51. KING, A I, YANG, K H, ZHANG, L and HARDY, W. 'Is head injury caused by linear or angular acceleration?' "Bertil Aldman award" Lecture, *Proc. IRCOBI Conf.,* 2003 1–12.

 doi:10.1533/ijcr.2004.0299

APPENDIX

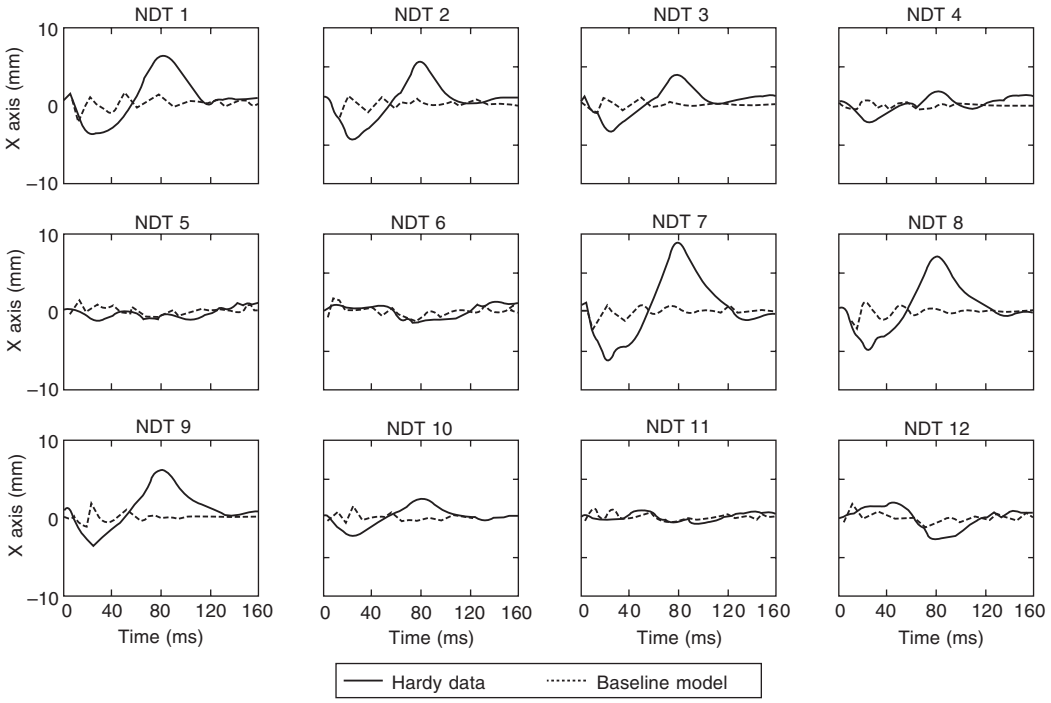

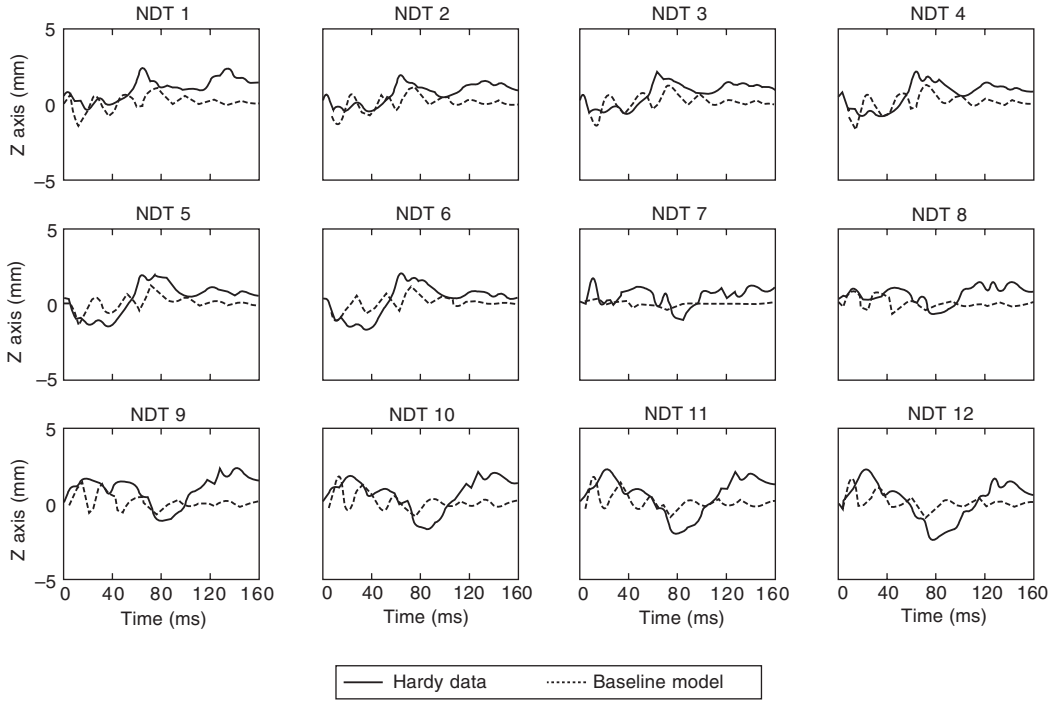

 doi:10.1533/ijcr.2004.0299

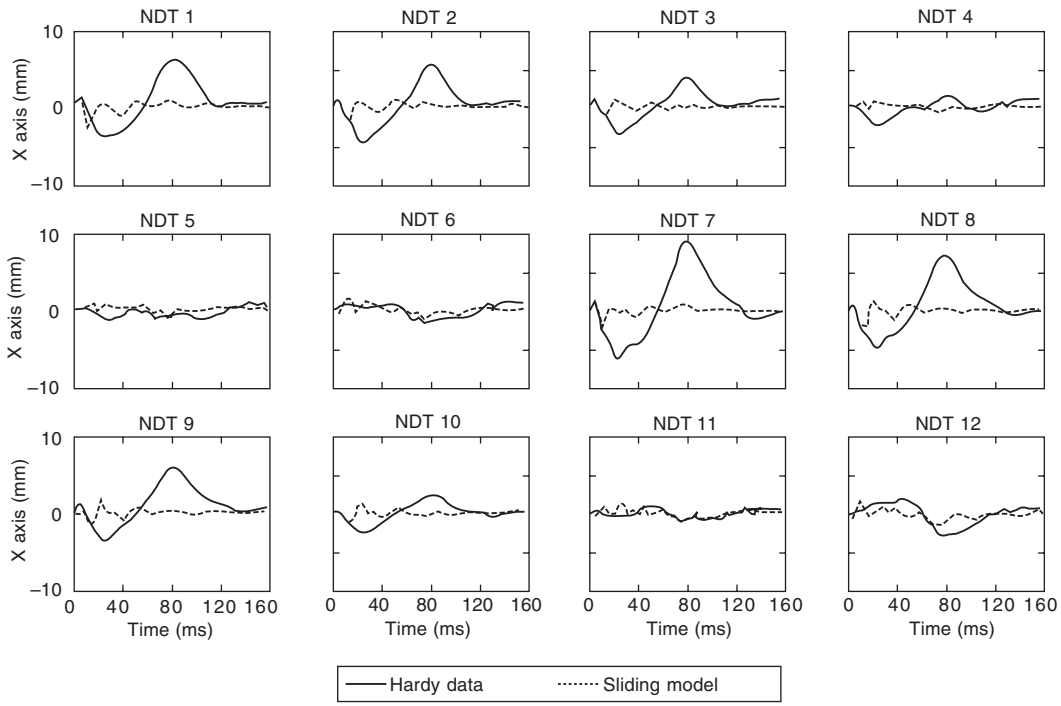
NDT 1
NDT 2
NDT 3
NDT 4
NDT 5
NDT 6
NDT 7
NDT 8
NDT 9
NDT 10
NDT 11
NDT 12
X axis (mm)
10
0
–10
0 40 80 120 160
Time (ms)
Hardy data
Sliding model

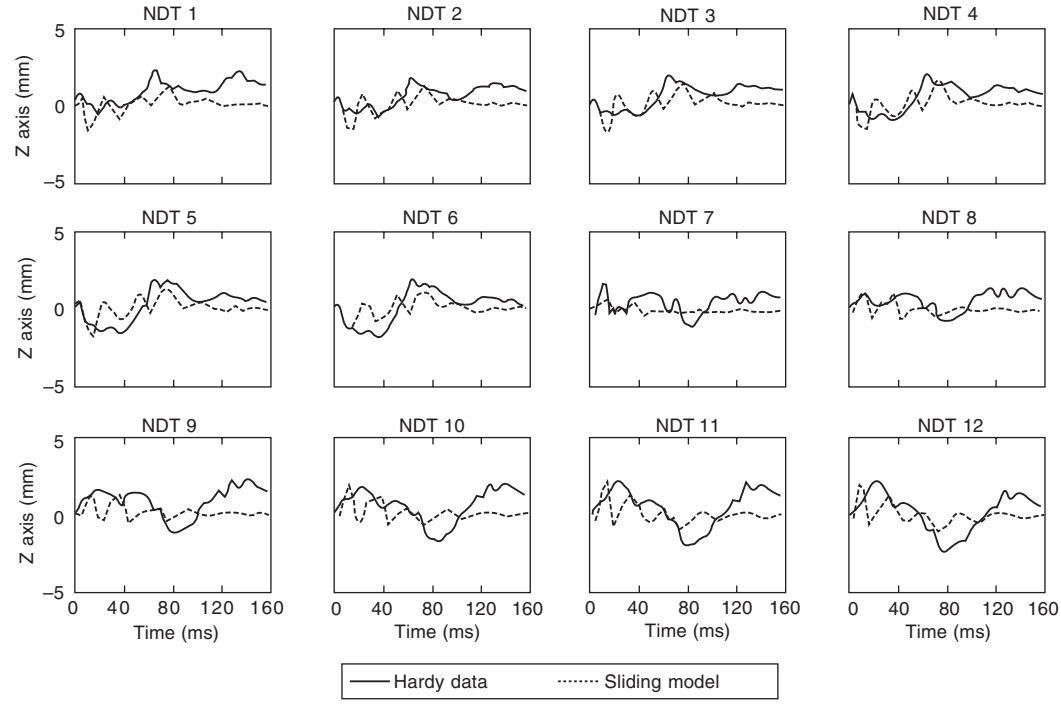
NDT 1
NDT 2
NDT 3
NDT 4
NDT 5
NDT 6
NDT 7
NDT 8
NDT 9
NDT 10
NDT 11
NDT 12
Z axis (mm)
5
0
–5
0 40 80 120 160
Time (ms)
Hardy data
Sliding model

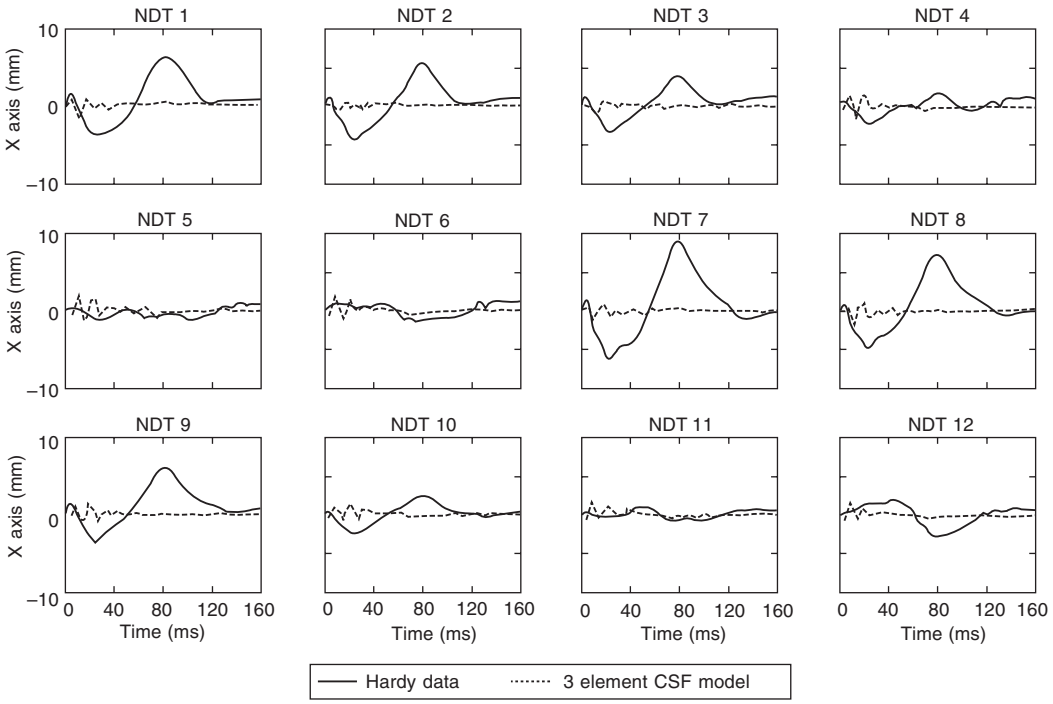

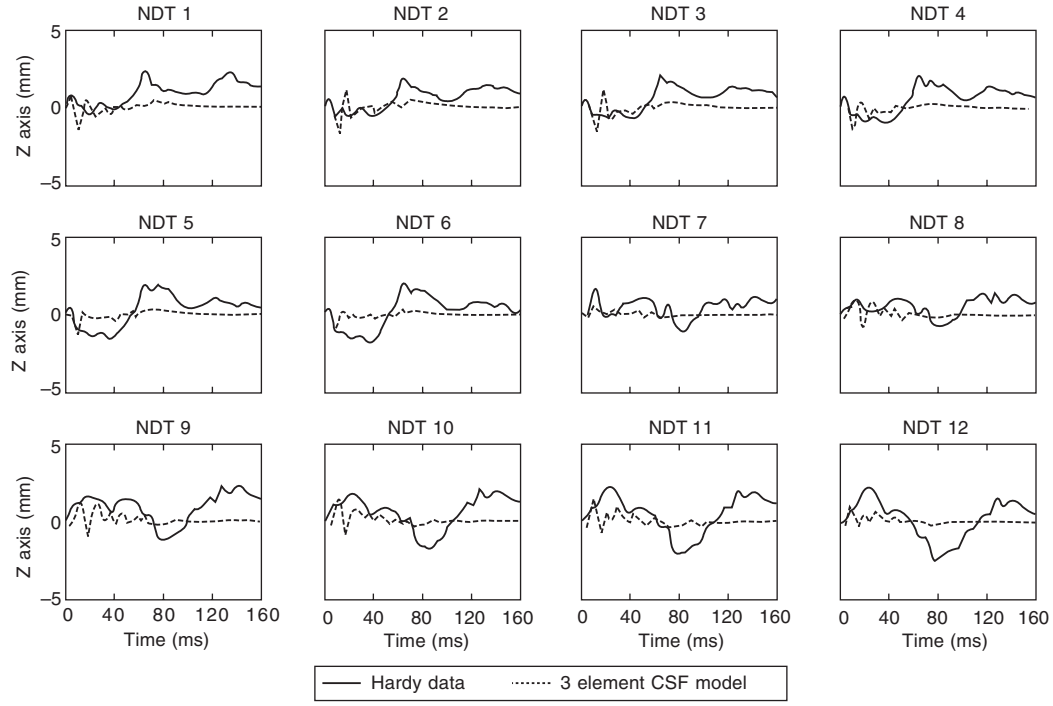

 doi:10.1533/ijcr.2004.0299

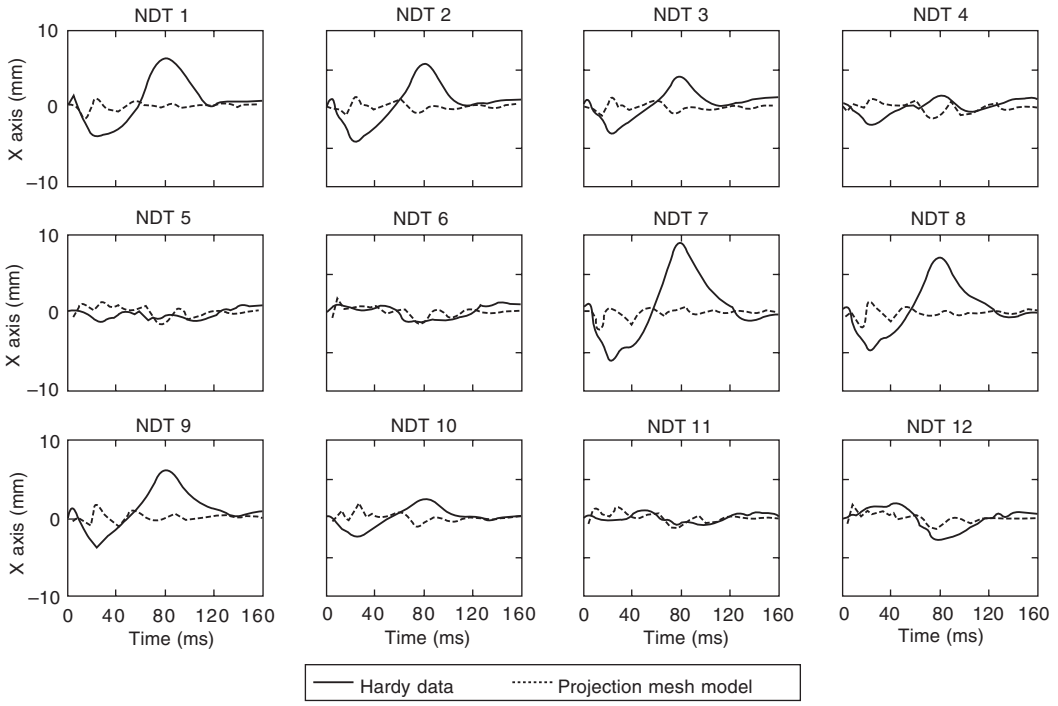
NDT 1
NDT 2
NDT 3
NDT 4
NDT 5
NDT 6
NDT 7
NDT 8
NDT 9
NDT 10
NDT 11
NDT 12
X axis (mm)
10
0
−10
0 40 80 120 160
Time (ms)
Hardy data
Projection mesh model

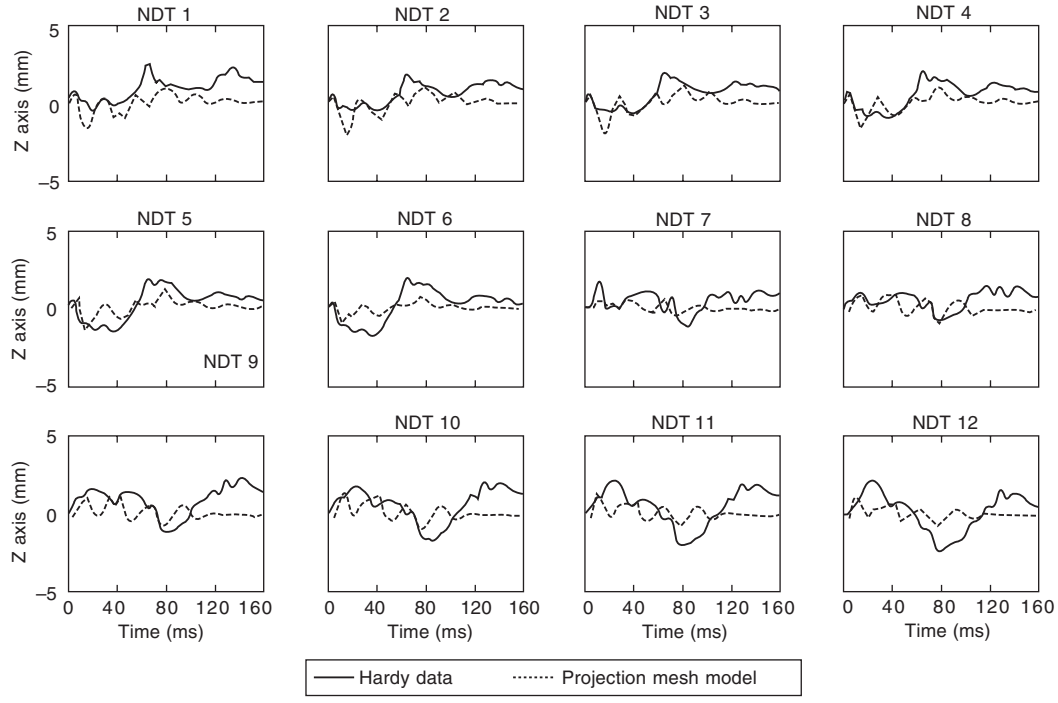
NDT 1
NDT 2
NDT 3
NDT 4
NDT 5
NDT 6
NDT 7
NDT 8
NDT 9
NDT 10
NDT 11
NDT 12
Z axis (mm)
5
0
−5
0 40 80 120 160
Time (ms)
Hardy data
Projection mesh model

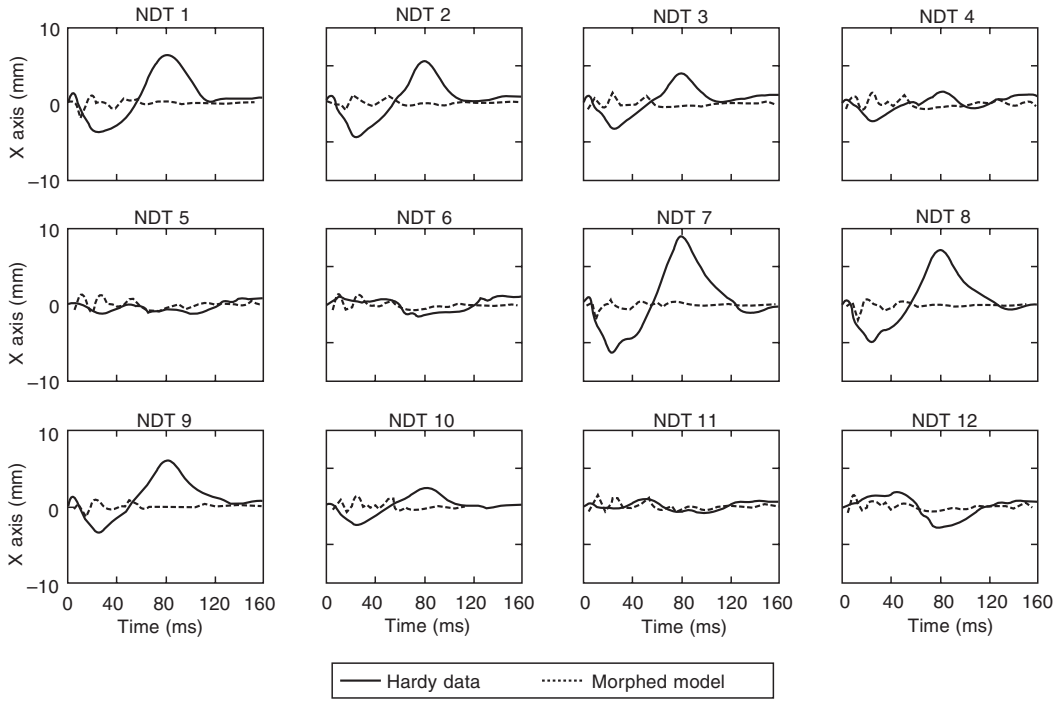

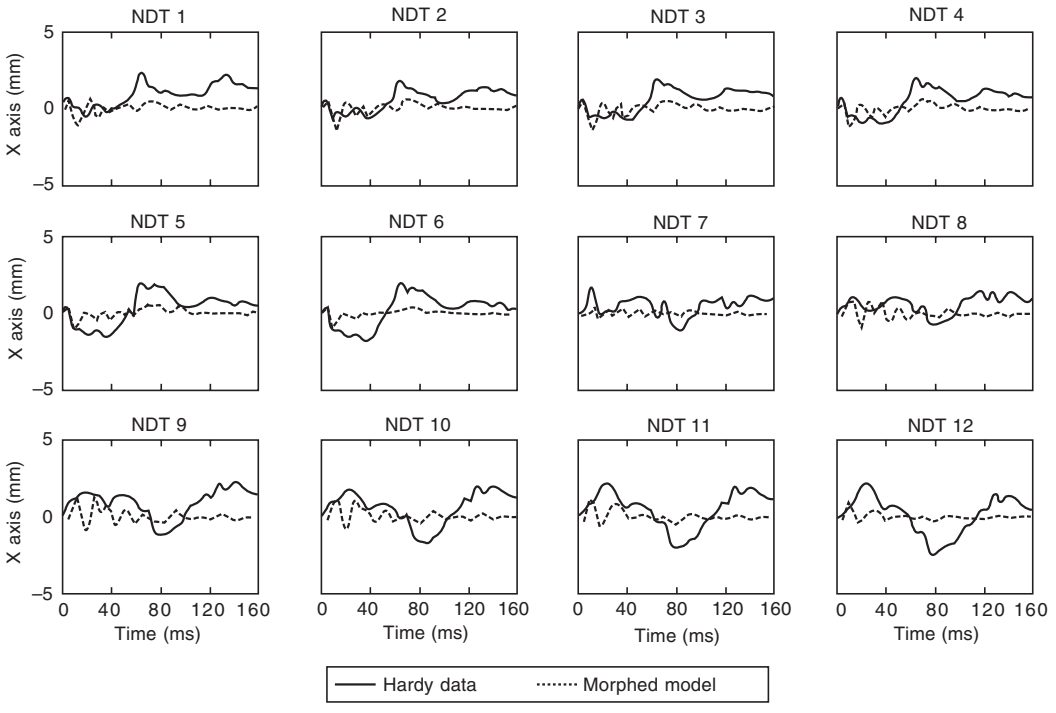

 doi:10.1533/ijcr.2004.0299